

000
001
002054
055
056

External Patch Group Prior Guided Internal Orthogonal Dictionary Learning for Real Image Denoising

057
058
059003
004
005
006
007060
061
062
063

Anonymous CVPR submission

008
009
010
011
012064
065
066
067

Paper ID ****

013
014
015068
069
070

Abstract

016
017
018
019
020071
072
073
074

For image denoising problem, the external and internal priors are playing key roles in many different methods. External priors learn from external images to restore noisy images while internal ones exploit priors of given images for denoising. The external priors are more generative and efficient on recovering structures existing in most images while the internal priors are more adaptive on recovering details existed in given noisy images. In this paper, we propose to employ the external patch group prior of images to guide the clustering of internal patch groups, and develop an external dictionary guided internal orthogonal dictionary learning algorithm for real image denoising. The internal orthogonal dictionary learning process has closed-form solutions and hence very efficient for online denoising. The experiments on standard datasets demonstrate that, that the proposed method achieves better performance than other state-of-the-art methods on real image denoising.

033
034
035075
076
077

1. Introduction

036
037
038
039
040078
079
080
081
082

Most vision systems, such as medical imaging and surveillance, need accurate feature extraction from high-quality images. The camera sensors and outdoor low light conditions will unavoidably bring noise to the captured images. The impact is that the image details will be lost or hardly visible. As a result, image denoising is an essential procedure for the reliability of these vision systems. In the research area, image denoising is also an ideal platform for testing natural image models and provides high-quality images for other computer vision tasks such as image registration, segmentation, and pattern recognition, etc.

041
042
043
044
045
046
047
048
049
050
051
052
053083
084
085
086
087
088
089
090
091
092
093
094
095
096
097
098
099
100
101
102
103
104
105
106
107

For several decades, there emerge numerous image denoising methods [1, 2, 3, 4, 5, 6, 7, 8, 9, 10, 11], and all of them focus mainly on dealing with additive white Gaussian noise (AWGN). In real world, the cameras will undertake high ISO settings for high-speed shots on actions, long exposure for low light on night shots, etc. Under these

situations, the noise is generated in a complex form and also been changed during the in-camera imaging pipeline [12, 13]. Therefore, the noise in real images are much more complex than Gaussian [13, 14]. It depends on camera series, brands, as well as the settings (ISO, shutter speed, and aperture, etc). The models designed for AWGN would become much less effective on real noisy images.

In the last decade, the methods of [15, 16, 17, 18, 19, 20, 13] are developed to deal with real noisy images. Almost all these methods employ a two-stage framework: estimating the parameters of the assumed noise model (usually Gaussian) and performing denoising with the help of the noise modeling and estimation in the first stage. However, the Gaussian assumption is inflexible in describing the complex noise on real noisy images [17]. Although the mixture of Gaussians (MoG) model is possible to approximate any noise distribution [21], estimating its parameters is time consuming via nonparametric Bayesian techniques [20]. To evaluate the performance of these methods on dealing with complex real noise, we apply these methods, with corresponding default parameters, on a real noisy image provided in [13]. The testing image is captured by a Nikon D800 camera when ISO is 3200. The "ground truth" image is also provided with which we can calculate objective measurements such as PSNR and SSIM [22]. The denoised images are listed in Figure 1, from which we can see that these methods either remove the noise or oversmooth the complex details in real noisy image.

The above mentioned methods can be categorized into external methods which learn priors from external images to recover noisy images, and internal ones which exploit priors of given images for denoising. The external priors in natural images are free of the high correlation between noise and signals in real noisy images, while the internal prior is adaptive to the image and can recover better the latent clean image. Combining the priors of external clean images and adaptively of internal testing images can naturally improve the performance of denoising methods, especially on real noisy images. Based on these observations, in this paper, we propose to employ the external patch group prior [10]

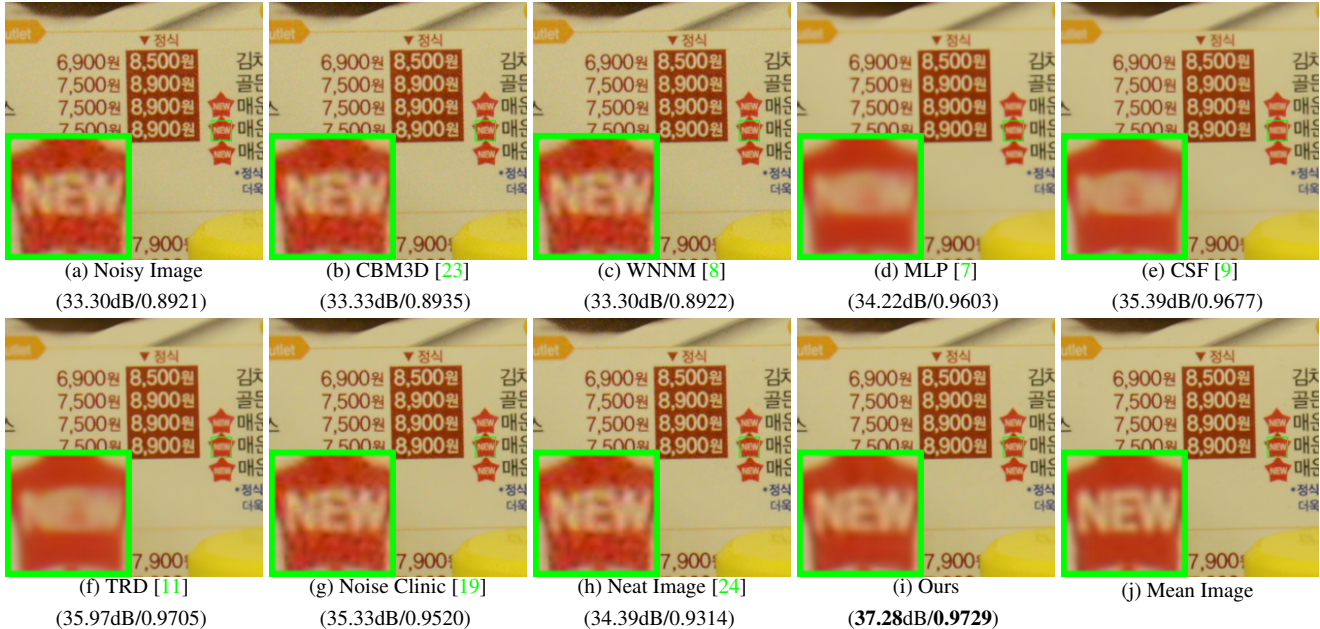


Figure 1. Denoised images of the real noisy image "Nikon D800 ISO 3200 A3" from [13] by different methods. The images are better viewed by zooming in on screen.

of natural clean images to guide the clustering of internal patch groups in given noisy image, and develop an external prior guided internal orthogonal dictionary learning (DL) algorithm for real image denoising. The internal orthogonal DL process includes two alternating stages: updating sparse coefficients and updating orthogonal dictionary. Both of the two stages have closed-form solutions. Hence, our internal DL process is very efficient for online internal denoising. Through comprehensive experiments on real noisy images captured by different cameras and settings, we demonstrate that the proposed method achieves better performance on real image denoising

1.1. Our Contributions

The contributions of this paper are summarized as follows:

- We propose a novel dictionary learning method which employ the external prior guided the internal orthogonal dictionary learning for real image denoising. Both the external prior and internal prior are performed on patch groups instead of patches.
- The internal orthogonal dictionary learning are alternating iterative solved with closed-form solutions. The learned orthogonal dictionary are very efficient in both learning and denoising stages.
- We achieve much better performance on the real image denoising problem than other competing methods in terms of visual quality, PSNR, and SSIM.

The rest of this paper will be summarized as follows: in Section 2, we will introduce the related work; in Section 3, we will introduce the proposed external prior guided internal orthogonal dictionary learning algorithm for real image denoising; in Section 4, we will demonstrate the extensive experiments on two standard dataset; we will conclude our paper and give our future work in Section 5.

2. Related Work

2.1. Patch Group Prior of Natural Images

The Patch Group (PG) prior [10] is proposed to directly model the non-local self similar (NSS) property of natural images. The NSS property is commonly used in image restoration tasks [1, 4, 5, 8, 10]. The PG prior largely reduces the space of images to be modeled when compared to the patch prior [6]. In [10], only the PGs of clean natural images is utilized, while the PGs of noisy input images are ignored. In this paper, we make use of PGs both from external clean images and internal given real noisy image for better denoising performance.

2.2. Internal v.s. External Dictionary Learning

Learning dictionaries to represent images has been successfully used in image modeling [3, ?, 6, 25, 33, 10]. There are mainly two categories of DL methods: 1) External DL methods pre-learned dictionary from a set of clean image patches, and the learned dictionaries are used to encode the noisy image patches for denoising [?, 6, 10]. 2) Internal DL methods directly learned dictionary from the patches of given noisy image, and the image denoising is simultane-

ously done with the DL process [3, 25, 33]. The external DL methods is not adaptive to the noisy image, while the internal DL methods is adaptive to the degraded images but it ignores the information hidden in clean images. In this paper, our goal is to employ the external dictionary to guide the learning of internal orthogonal dictionary.

2.3. Real Image Denoising

In the last decade, there are many methods [15, 16, 17, 18, 19, 20, 13] proposed for real image denoising problem. In the seminar work of BLS-GSM [30] for real image denoising, Portilla et al. proposed to use scale mixture of Gaussian in overcomplete oriented pyramids to estimate the latent clean images. In [15], Portilla proposed to use a correlated Gaussian model for noise estimation of each wavelet subband. The work of Rabie [16] modeled the noisy pixels as outliers which are removed via Lorentzian robust estimator [31]. Liu et al. [17] proposed to use 'noise level function' (NLF) to estimate the noise and then use Gaussian conditional random field to obtain the latent clean image. Gong et al. [18] models the noise by mixed ℓ_1 and ℓ_2 norms and remove the noise by sparsity prior in the wavelet transform domain. Later, Lebrun et al. proposed a multi-scale denoising algorithm called 'Noise Clinic' [19]. This method generalizes the NL-Bayes model [32] to deal with blind noise and achieves state-of-the-art performance. Recently, Zhu et al. proposed a Bayesian model [20] which approximates and remove the noise via Low-Rank Mixture of Gaussians (LR-MoG). The commercial software Neat Image [24] first estimates the parameters of noise via a large flat area and then filters the noise accordingly.

3. External Patch Group Prior Guided Internal Orthogonal Dictionary Learning

In this section, we formulate the framework of external patch group (PG) prior guided internal orthogonal dictionary learning. We first introduce the patch PG leaning on clean natural RGB images. Then we propose to employ the external PG prior to guide the internal clustering and orthogonal dictionary learning (DL). The orthogonal DL has alternative closed-form solutions in term of updating sparse coefficients and dictionary. Finally, we discuss the advantages of our proposed external PG prior guided internal orthogonal dictionary learning algorithm.

3.1. External Patch Group Prior Learning

Natural images often demonstrate repetitive local patterns, this nonlocal self-similarity (NSS) property is a key successful factor for many image denoising methods [1, 4, 5, 33, 8, 10]. In this section, we formulate the Patch Group prior learned on natural color images. Similar to [10], the patch group (PG) is defined as a group of simi-

lar patches to the local patch. The patch group mean is distracted, and hence different groups patches can share similar PGs. In this way, the space natural image patches to be modeled is largely reduced. In this work, each local patch extracted from RGB images is of size $p \times p \times 3$. Then we search the M most similar patches $\{\mathbf{x}_m\}_{m=1}^M$ around each local patch through Euclidean distance, in a local window of size $W \times W$. The $\mathbf{x}_m \in \mathbb{R}^{3p^2 \times 1}$ is a patch vector formed by combining the 3 patch vectors (of size $p^2 \times 1$) in R, G, B channels. The mean vector of this PG is $\boldsymbol{\mu} = \frac{1}{M} \sum_{m=1}^M \mathbf{x}_m$, and the group mean subtracted PG is defined as $\bar{\mathbf{X}} \triangleq \{\bar{\mathbf{x}}_m = \mathbf{x}_m - \boldsymbol{\mu}\}, m = 1, \dots, M$. Assume we have extracted N PGs from a set of external natural images, and the n -th PG is defined as $\bar{\mathbf{X}}_n \triangleq \{\bar{\mathbf{x}}_{n,m}\}_{m=1}^M, n = 1, \dots, N$. We employ the Gaussian Mixture Model (GMM) to learn the external patch group based NSS prior. In this model, the likelihood of the n -th PG $\{\bar{\mathbf{X}}_n\}$ can be calculated as

$$P(\bar{\mathbf{X}}_n) = \sum_{k=1}^K \pi_k \prod_{m=1}^M \mathcal{N}(\bar{\mathbf{x}}_{n,m} | \boldsymbol{\mu}_k, \boldsymbol{\Sigma}_k), \quad (1)$$

where K is the number of Gaussians and the k -th Gaussian is $\{\mathcal{N}(\boldsymbol{\mu}_k, \boldsymbol{\Sigma}_k)\}$. By assuming that all the PGs are independently sampled, the overall objective log-likelihood function is

$$\ln \mathcal{L} = \sum_{n=1}^N \ln \left(\sum_{k=1}^K \pi_k \prod_{m=1}^M \mathcal{N}(\bar{\mathbf{x}}_{n,m} | \boldsymbol{\mu}_k, \boldsymbol{\Sigma}_k) \right). \quad (2)$$

We maximize the above objective function for PG-GMM learning and finally obtain the GMM model with learned parameters including mixture weights $\{\pi_k\}_{k=1}^K$, mean vectors $\{\boldsymbol{\mu}_k = \mathbf{0}\}_{k=1}^K$, and covariance matrices $\{\boldsymbol{\Sigma}_k\}_{k=1}^K$. Noted that the mean vector of each cluster is natural zeros, i.e., $\boldsymbol{\mu}_k = \mathbf{0}$.

3.2. External Prior Guided Internal Orthogonal Dictionary Learning

Given a rael noisy image, we extract noisy PGs from it and save the mean vectors of each PG for recovering. The mean substracted PG is defined as $\bar{\mathbf{Y}}$. To project this PG into a most adaptive subspace, we select the most suitable Gaussian component to it from the PG-GMM trained in previous section. The selection can be done by checking the posterior probability that $\bar{\mathbf{Y}}$ belongs to the k th Gaussian component:

$$P(k|\bar{\mathbf{Y}}) = \frac{\prod_{m=1}^M \mathcal{N}(\bar{\mathbf{y}}_m | \mathbf{0}, \boldsymbol{\Sigma}_k)}{\sum_{l=1}^K \prod_{m=1}^M \mathcal{N}(\bar{\mathbf{y}}_m | \mathbf{0}, \boldsymbol{\Sigma}_l)}. \quad (3)$$

Since the noise on real images are mostly small when compared to the signals, the covariance matrix of the k th component is still $\boldsymbol{\Sigma}_k$. Finally, the component with the maximum A-posteriori (MAP) probability $\ln P(k|\bar{\mathbf{Y}})$ is selected as the most suitable subspace for $\bar{\mathbf{Y}}$.

Though each PG has been projected into its most suitable subspace, the pre-learned subspace is still too general to

324 represent the noisy PG extracted from the real noisy image.
 325 That is, the noisy PGs projected into one cluster can still
 326 constisted a subspace which is of lower dimensions than the
 327 subspace pre-learned from the external PGs. This can be
 328 demonstrated by compare the distribution of external PGs
 329 and internal PGs in the same clusters. We randomly select
 330 one cluster, and collect the celan PGs extracted from exter-
 331 nal dataset (Kodak 24 images) and the niosy PGs from the
 332 testing image. Since the original PGs are of $3p^2$ dimensions,
 333 we apply PCA to project the PGs into 2 dimensions for bet-
 334 ter visualization. The results is shown in Figure ??, from
 335 which we can see clearly that the projected PGs are mainly
 336 in a smaller region of the external PGs, which proves that
 337 the internal PGs are only consisted a subspace in a lower
 338 dimension than the PGs collected from external subspace.
 339 To better and adaptively charactering the internal PGs from
 340 the testing image, we need learn a more specific dictionary
 341 for noisy PGs assigned into each cluster. For notation sim-
 342 plicity, we ignore the index of subspace k . The internal PGs
 343 \mathbf{Y} form a subspace which can be obtained by singular value
 344 decomposition (SVD),
 345

$$\begin{aligned} & \min_{\mathbf{D}_i \in \mathbb{R}^{3p^2 \times r}, \mathbf{A} \in \mathbb{R}^{3p^2 \times MN}} \|\mathbf{Y} - [\mathbf{D}_e \mathbf{D}_i] \mathbf{A}\|_F^2 + \lambda \|\mathbf{A}\|_1 \\ & \text{s.t. } \mathbf{D}_i^T \mathbf{D}_i = \mathbf{I}_r, \mathbf{D}_e^T \mathbf{D}_i = \mathbf{0}, \end{aligned} \quad (4)$$

The singular vectors capture the statistical structures of NSS variations in natural images, while the singular values in \mathbf{S} represent the significance of these singular vectors. Fig. 4 shows the singular vectors for one Gaussian component.

3.3. Optimization with Closed-form Solution

Similar to the K-SVD [3], we employ an alternating iterative framework to solve the optimization problem 4. In fact, we initialize the orthogonal dictionary as $\mathbf{D}^{(0)}$ and for $t = 0, 1, \dots, T - 1$, alternatively do

Updating Sparse Coefficients: given the initialization orthogonal dictioany $\mathbf{D}_i^{(t)}$, the sparce coefficients $\mathbf{A}^{(t)}$ are obtained via solving

$$\mathbf{A}^{(t)} := \arg \min_{\mathbf{A} \in \mathbb{R}^{3p^2 \times MN}} \|\mathbf{Y} - [\mathbf{D}_e \mathbf{D}_i^{(t)}] \mathbf{A}\|_F^2 + \lambda \|\mathbf{A}\|_1. \quad (5)$$

This problem has closed-form solution by $\mathbf{A}^* = T_\lambda(\hat{\mathbf{D}}^T \mathbf{Y})$, where $T_\lambda(\mathbf{A}) = \text{sgn}(\mathbf{A}) \odot \max(\mathbf{A}, \lambda)$ is a soft-thresholding function.

Updating Orthogonal Dictionary: given the sparse coefficients $\mathbf{A}^{(0)}$, the sparce coefficients $\mathbf{A}^{(t)}$ are obtained via solving

$$\begin{aligned} \mathbf{D}_i^{(t+1)} &:= \arg \min_{\mathbf{D}_i \in \mathbb{R}^{3p^2 \times r}} \|\mathbf{Y} - [\mathbf{D}_e \mathbf{D}_i] \mathbf{A}^{(t)}\|_F^2 \\ &\text{s.t. } \mathbf{D}_i^T \mathbf{D}_i = \mathbf{I}_r, \mathbf{D}_e^T \mathbf{D}_i = \mathbf{0}, \end{aligned} \quad (6)$$

Dividing the sparse coefficients $\mathbf{A} = [\mathbf{A}_e^T \mathbf{A}_i^T]^T$, where \mathbf{A}_e and \mathbf{A}_i denote the coefficients over external and internal

378 dictionary \mathbf{D}_e and \mathbf{D}_i . According to the Proposition 2.2
 379 in [34], the problem (6) has a closed-form solution $\mathbf{D}_i^* =$
 380 $\mathbf{U} \mathbf{V}^T$, where \mathbf{U} and \mathbf{V} are the orthogonal matrices obtained
 381 by the following SVD
 382

$$(\mathbf{I} - \mathbf{D}_e \mathbf{D}_e^T) \mathbf{Y} \mathbf{A}_i^T = \mathbf{U} \Sigma \mathbf{V}^T \quad (7)$$

With these solutions, the final obtained dictionary $\mathbf{D} = [\mathbf{D}_e \mathbf{D}_i]$ are orthogonal ictionary. This can be proved by the following equation

$$\mathbf{D}^T \mathbf{D} = \left(\begin{array}{c} \mathbf{D}_e^T \\ \mathbf{D}_i^T \end{array} \right) (\mathbf{D}_e \mathbf{D}_i) = \left(\begin{array}{c} \mathbf{D}_e^T \mathbf{D}_e & \mathbf{D}_e^T \mathbf{D}_i \\ \mathbf{D}_i^T \mathbf{D}_e & \mathbf{D}_i^T \mathbf{D}_i \end{array} \right) = \mathbf{I} \quad (8)$$

3.4. Discussion on External Prior and Internal Orthogonal Dictionary Learning

Until now, we have divided the noisy PGs into multiple internal subspaces. Here we take a deep analysis on how the external NSS prior guide the subspace learning of internal PGs. The help are at least threefold. Firstly, through MAP in (3), the external prior guides the noisy PGs to be clustered into the correct subspaces. If we cluster the noisy PGs in an automatical way, the subspaces we learned will be highly degraded by the signal dependent noise. Secondly, the guidance of external prior for internal clustering is more efficient than directly clustering the internal noisy PGs. It only needs to calculate the MAP probability via the equation (3) while the internal clustering via GMM is time-consuming on EM algorithm [35]. Thirdly, due to the correct guidance of external prior, the structural decomposition via SVD of each subspace is more adaptive. This will bring better denoising performance than the methods only using the external information. The *mutual incoherence* $\mu(\mathbf{U})$ [36], which is difined as

$$\mu(\mathbf{U}) = \max_{i=j} \frac{|\mathbf{d}_i^T \mathbf{d}_j|}{\|\mathbf{d}_i\|_2 \|\mathbf{d}_j\|_2} \quad (9)$$

, is a measure of quality of dictionary.

The Internal PGs are in fact lying in the subspaces of external PG Spaces. To defend this argument, we compare the distribution of external PGs extracted from clean natural images and real noisy images. For better illumination, we randomly selected a cluster and project the original clean PGs \mathbf{X} onto a 2-D plane. This could be done via $\mathbf{X}_p = \mathbf{U}(:, 1 : 2)^T \mathbf{X}$, where \mathbf{U} is the singular vector matrix of that cluster. The noisy PGs \mathbf{Y} assigned in this cluster is also projected into 2-D via $\mathbf{Y}_p = \mathbf{U}(:, 1 : 2)^T \mathbf{Y}$. The Figure ?? reflects the distribution on the 2-D plane of the projected clean PGs from external natural images and the projected noisy PGs from internal image. We can see that the internal noisy PGs are indeed lying in a subspace of the external PGs. Hence, if we directly use the external prior learned from clean PGs, the learned subspaces would be too generative to be suitable for the testing data.

432 Through SVD, the PGs in each internal subspace can be
 433 divided into singular vectors and singular values. The singular
 434 vectors are the basis of the corresponding subspace
 435 while the singular values reflect the importance of these basis.
 436 The basis can be used as dictionary to code the noisy
 437 PGs. And the singular values are adaptive parameters for
 438 internal noisy PGs. We can compare the singular values of
 439 one internal subspace and the corresponding space of external
 440 PGs. The result is shown in Figure ???. From which we
 441 can see that the noisy subspace often have higher values
 442 than external space consisted of clean PGs. This gap is
 443 clearly made of the noise and can be used for image denoising
 444 in a natural way.

4. The Denoising Algorithm

4.1. Fast Patch Group Searching by Integral Image

450 The searching of patch groups in images is inefficient if we search non-local similar patches to each local patch.
 451 To speed up the searching process and make our proposed
 452 method faster, we employ the technique of 'Summed Area
 453 Table' [37] for efficient PG searching. The SAT permits
 454 to evaluate the sum of pixel values in rectangular regions
 455 of the image with four operations, regardless of the region
 456 size. That is to say, we do not need do distance measure for
 457 each patch. It was first proposed under the name of summed
 458 area table[38].

4.2. Prior Weights for Sparse Coding

460 To remove the real noise, we employ the sparse coding
 461 framework. And in order to be adaptive to the input image,
 462 we employ the internal learned \mathbf{U} of each cluster as
 463 an adaptive dictionary to represent the structural variations
 464 of the PGs in that cluster. Since the \mathbf{U} is orthonormal, its
 465 *mutual incoherence* is naturally 0 and therefore better than
 466 other redundant dictionaries.

$$\min_{\alpha} \|\bar{\mathbf{y}}_m - \mathbf{U}\alpha\|_2^2 + \sum_{i=1}^{3p^2} \lambda_i |\alpha_i|. \quad (10)$$

473 The i th entry of the regularization parameter λ_i

$$\lambda_i = \lambda / (\mathbf{S}_i + \varepsilon), \quad (11)$$

476 where ε is a small positive number to avoid dividing by zero.
 477 Since the dictionary \mathbf{U} is orthonormal, it is not difficult to
 478 find out that (4) has a closed-form solution (detailed derivation
 479 can be found in the supplementary material):

$$\hat{\alpha} = \text{sgn}(\mathbf{U}^T \bar{\mathbf{y}}_m) \odot \max(|\mathbf{U}^T \bar{\mathbf{y}}_m| - \Lambda, 0), \quad (12)$$

481 where $\Lambda = [\lambda_1, \lambda_2, \dots, \lambda_{3p^2}]$ is the vector of regularization
 482 parameter and $\text{sgn}(\bullet)$ is the sign function, \odot means
 483 element-wise multiplication, and $|\mathbf{U}^T \bar{\mathbf{y}}_m|$ is the absolute
 484 value of each entry of vector $|\mathbf{U}^T \bar{\mathbf{y}}_m|$. The closed-form

Alg. 1: External Prior Guided Internal Orthogonal Dictionary Learning for Denoising	486 487 488 489 490 491 492 493 494 495 496 497 498 499 500 501 502 503 504 505 506 507 508 509 510 511 512 513 514 515 516 517 518 519 520 521 522 523 524 525 526 527 528 529 530 531 532 533 534 535 536 537 538 539
Input: Noisy image \mathbf{y} , PG-GMM model	#****
1. Initialization: $\hat{\mathbf{x}}^{(0)} = \mathbf{y}, \mathbf{y}^{(0)} = \mathbf{y}$;	#****
for $t = 1 : IteNum$ do	#****
for each PG \mathbf{Y} do	#****
2. Calculate group mean μ_y and form PG $\bar{\mathbf{Y}}$;	#****
3. Gaussian component selection via (3);	#****
end for	#****
for each Internal Subspace do	#****
4. Internal Subspace Learning by (4);	#****
5. Recover each patch in all PGs via $\hat{\mathbf{x}}_m = \mathbf{D}\hat{\alpha} + \mu_y$;	#****
end for	#****
6. Aggregate the recovered PGs of all subspaces to form the recovered image $\hat{\mathbf{x}}^{(t)}$;	#****
end for	#****
Output: The recovered image $\hat{\mathbf{x}}^{(IteNum)}$.	#****



Figure 2. Some testing images in the dataset [13].

solution makes our weighted sparse coding process very efficient.

4.3. The Overall Algorithm

With the solution $\hat{\alpha}$ in (7), the clean patch in a PG can be estimated as $\hat{\mathbf{x}}_m = \mathbf{D}\hat{\alpha} + \mu_y$. Then the clean image can be reconstructed by aggregating all the estimated PGs. In practice, we could perform the above denoising procedures for several iterations for better denoising outputs. In iteration t , we use the iterative regularization strategy [39] to add back to the recovered image $\hat{\mathbf{x}}^{(t-1)}$ some estimation residual in iteration $t-1$. The proposed denoising algorithm is summarized in Algorithm 1 (Alg. 1).

5. Experiments

In this section, we perform real image denoising experiments on three standard datasets. The first dataset is real noisy images with mean images as ground truths provided by [13], some samples are shown in Figure 3. The second dataset is provided by the website of Noise Clinic [19]. The third dataset is provided by the Commercial software Neat Image [24]. The second and third dataset do not have ground truth images.



Figure 3. Some cropped images of the dataset [13].

Table 1. Average PSNR(dB)/SSIM results of external, internal, and guided methods on 60 cropped real noisy images in [13].

	Noisy	Offline	Online	Guided
PSNR	34.51	38.19	38.07	38.55
SSIM	0.8718	0.9663	0.9625	0.9675

5.1. Implementation Details

Our proposed method contains two stages, the external prior guided internal subspace learning stage and the adaptive denoising stage. In the learning stage, there are 4 parameters: the patch size p , the number of patches in a PG M , the window size W for PG searching and the number of clusters K . We set $p = 6$ (hence the patch size is $6 \times 6 \times 3$), $M = 10$, $W = 31$, $K = 32$. We extracted about 3.6 million PGs from the Kodak PhotoCD Dataset, which includes 24 high quality color images, to train the external prior via PG-GMM. In the denoising stage, the parameter $\lambda = 0.002$ is used to regularize the sparse term. The δ in iterative regularization is set as $\delta = 0.09$.

5.2. Comparison on External and Internal methods

In this subsection, we compared the proposed external prior guided internal subspace learning model on real image denoising. The three methods are evaluated on the dataset provided in [13]. We calculate the PSNR, SSIM [22] and visual quality of these three methods. We also compare the speed. The PSNR and SSIM results on 60 cropped images from [13] are listed in Table 1. The images are cropped into size of 500×500 for better illustration. We also compare the three methods on visual quality in Figure 5.2. Compare the denoised images listed in Figure 5.2 and Figure 5.2, we can see that the Offline method is better at edges, smooth regions while the Online method is good at complex textures. The reason is two folds. Firstly, the Offline method is learned on clean images and hence is better at representing edges, structures, and smooth area. The online method is influenced by the noise and hence some noise cannot be removed. Secondly, the Online method is better at recovering complex area since they could learn adaptive dictionaries for the specific area. The Offline method cannot recover the complex area since they did not learn the similar structures from the external natural clean images.

5.3. Comparison With other Competing Methods

We compare with previous state-of-the-art Gaussian noise removal methods such as BM3D [4], WNNM [8], MLP [7], CSF [9], and the recently proposed TRD [11]. We also compare with three competing real image denoising methods such as Noise Clinic, Neat Image, and the CCNoise method proposed recently. The popular software NeatImage which is one of the best denoising software available. All these methods need noise estimation which is very hard to perform if there is no uniform regions available in the testing image. The NeatImage will fail to perform automatical parameters settings if there is no uniform regions.¹

We the competing denoising methods from various research directions on two datasets. Both the two datasets comes from the [13]. The first dataset contains 17 images of size over 7000×5000 . Since this dataset contains repetitive contents across different images, we crop 60 small images of size 500×500 from these 17 images in [13].

The PSNR and SSIM resluts are listed in Table 3. The number in red color and blue color means the best and second best results, respectively. From the Table 3, we can see that the external based method can already surpass largely the previous denoising methods. The improvement on PSNR over the second best method, i.e., TRD, is 0.44dB. The

5.4. Discussion on Parameter λ

The proposed method only has a key parameter, namely the regularization paramters λ . To demonstrate that the proposed method is robust to the variance of λ , we vary the parameter λ across a wide range and obtain the PSNR and SSIM results as a function of the parameter λ . The results is shown in Figure 8, from which we can see that the proposed method can achieve a PSNR (SSIM) over 38.5dB (0.9660) when λ varies from 0.0015 to 0.0025. This shows that the proposed method is indeed robust to the chosen of the paramter λ .

6. Conclusion and Future Work

In the future, we will evaluate the proposed method on other computer vision tasks such as single image super-resolution, photo-sketch synthesis, and cross-domain image recognition. Our proposed method can be improved if we use better training images, fine tune the parameters via cross-validation. We believe that our framework can be useful not just for real image denoising, but for image super-resolution, image cross-style synthesis, and recognition tasks. This will be our line of future work.

¹To compare with CCNoise, we first transform the denoised images into double format.

648

649

650

651

652

653

654

655

656

657

658

659

660

661

662

663

664

665

666

667

668

669

670

671

672

673

674

675

676

677

678

679

680

681

682

683

684

685

686

687

688

689

690

691

692

693

694

695

696

697

698

699

700

701

702

703

704

705

706

707

708

709

710

711

712

713

714

715

716

717

718

719

720

721

722

723

724

725

726

727

728

729

730

731

732

733

734

735

736

737

738

739

740

741

742

743

744

745

746

747

748

749

750

751

752

753

754

755



Figure 4. Denoised images of the image "Nikon D600 ISO 3200 C1" by different methods. The images are better to be zoomed in on screen.

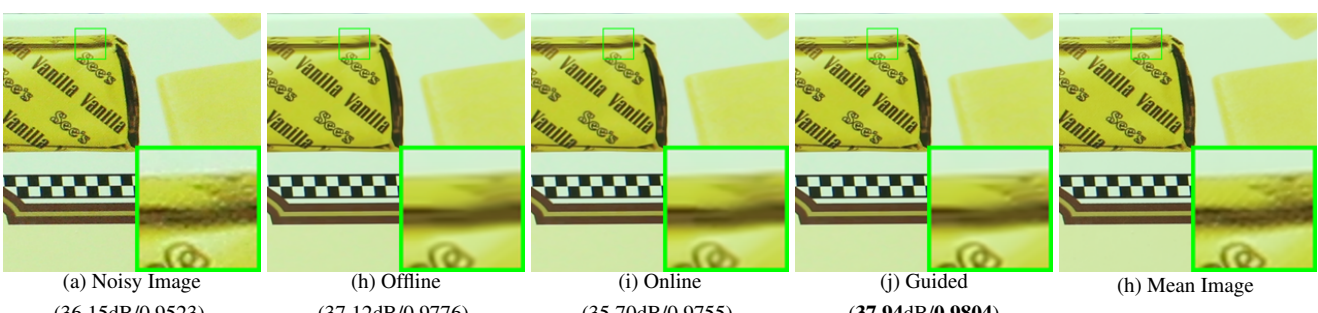


Figure 5. Denoised images of the image "Canon EOS 5D Mark3 ISO 3200 C1" by different methods. The images are better to be zoomed in on screen.

References

- [1] A. Buades, B. Coll, and J. M. Morel. A non-local algorithm for image denoising. *CVPR*, pages 60–65, 2005. [1](#), [2](#), [3](#)
- [2] S. Roth and M. J. Black. Fields of Experts. *International Journal of Computer Vision*, 82(2):205–229, 2009. [1](#)
- [3] M. Elad and M. Aharon. Image denoising via sparse and redundant representations over learned dictionaries. *Image Processing, IEEE Transactions on*, 15(12):3736–3745, 2006. [1](#), [2](#), [3](#), [4](#)
- [4] K. Dabov, A. Foi, V. Katkovnik, and K. Egiazarian. Image denoising by sparse 3-D transform-domain collaborative filtering. *Image Processing, IEEE Transactions on*, 16(8):2080–2095, 2007. [1](#), [2](#), [3](#), [6](#)
- [5] J. Mairal, F. Bach, J. Ponce, G. Sapiro, and A. Zisserman. Non-local sparse models for image restoration. *ICCV*, pages 2272–2279, 2009. [1](#), [2](#), [3](#)
- [6] D. Zoran and Y. Weiss. From learning models of natural image patches to whole image restoration. *ICCV*, pages 479–486, 2011. [1](#), [2](#)
- [7] Harold C Burger, Christian J Schuler, and Stefan Harmeling. Image denoising: Can plain neural networks compete with bm3d? *Computer Vision and Pattern Recognition (CVPR), 2012 IEEE Conference on*, pages 2392–2399, 2012. [1](#), [2](#), [6](#)
- [8] S. Gu, L. Zhang, W. Zuo, and X. Feng. Weighted nuclear norm minimization with application to image denoising. *CVPR*, pages 2862–2869, 2014. [1](#), [2](#), [3](#), [6](#)
- [9] U. Schmidt and S. Roth. Shrinkage fields for effective image restoration. *Computer Vision and Pattern Recognition (CVPR), 2014 IEEE Conference on*, pages 2774–2781, June 2014. [1](#), [2](#), [6](#)
- [10] J. Xu, L. Zhang, W. Zuo, D. Zhang, and X. Feng. Patch group based nonlocal self-similarity prior learning for image denoising. *2015 IEEE International Conference on Computer Vision (ICCV)*, pages 244–252, 2015. [1](#), [2](#), [3](#)
- [11] Yunjin Chen, Wei Yu, and Thomas Pock. On learning optimized reaction diffusion processes for effective image restoration. *Proceedings of the IEEE Conference on Computer Vision and Pattern Recognition*, pages 5261–5269, 2015. [1](#), [2](#), [6](#)
- [12] S. J. Kim, H. T. Lin, Z. Lu, S. Ssstrunk, S. Lin, and M. S. Brown. A new in-camera imaging model for color computer vision and its application. *IEEE Transactions on Pattern Analysis and Machine Intelligence*, 34(12):2289–2302, Dec 2012. [1](#)
- [13] Seonghyeon Nam, Youngbae Hwang, Yasuyuki Matsushita, and Seon Joo Kim. A holistic approach to cross-channel image noise modeling and its application to image denoising. *Proc. Computer Vision and Pattern Recognition (CVPR)*, pages 1683–1691, 2016. [1](#), [2](#), [3](#), [5](#), [6](#), [8](#)
- [14] Glenn E Healey and Raghava Kondepudy. Radiometric ccd camera calibration and noise estimation. *IEEE Transactions on Pattern Analysis and Machine Intelligence*, 16(3):267–276, 1994. [1](#)

756 Table 2. Average PSNR(dB) results of different methods on 60 cropped real noisy images captured in [13].
757

	Noisy	CBM3D	WNNM	MLP	CSF	TRD	NI	NC	Guided	Guided2
PSNR	34.51	34.58	34.52	36.19	37.40	37.75	36.53	37.57	38.72	38.90
SSIM	0.8718	0.8748	0.8743	0.9470	0.9598	0.9617	0.9241	0.9514	0.9694	0.9702

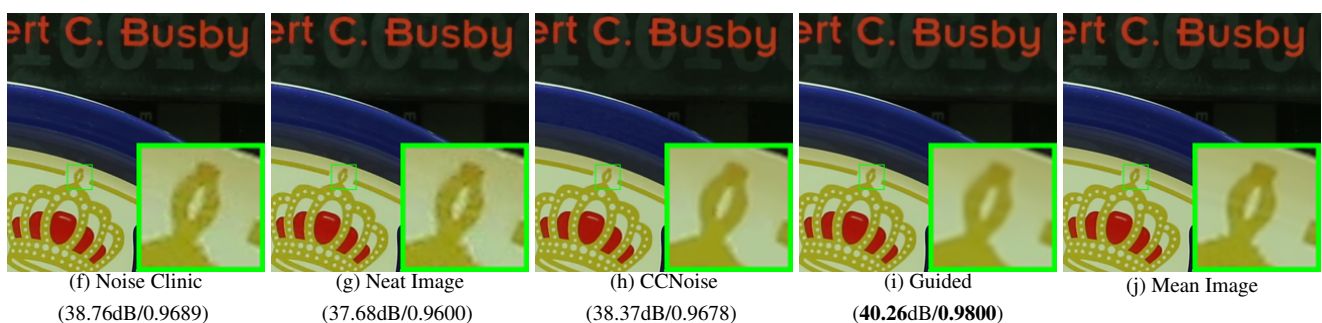
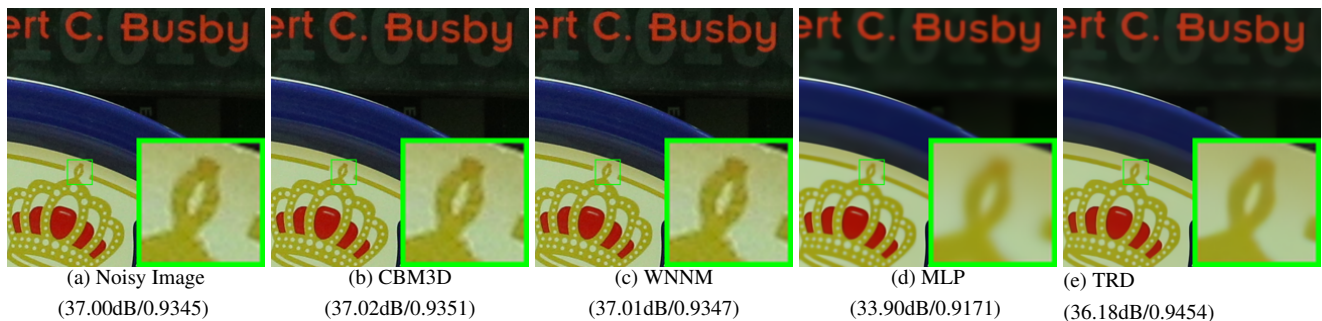
761 Table 3. Average PSNR(dB) results of different methods on 15 cropped real noisy images used in [13].
762

Camera Settings	Noisy	CBM3D	WNNM	MLP	CSF	TRD	NI	NC	CC	Guided2
Canon 5D Mark III ISO = 3200	37.00	37.08	37.09	33.92	35.68	36.20	37.68	38.76	38.37	40.50
	33.88	33.94	33.93	33.24	34.03	34.35	34.87	35.69	35.37	37.22
	33.83	33.88	33.90	32.37	32.63	33.10	34.77	35.54	34.91	37.13
Nikon D600 ISO = 3200	33.28	33.33	33.34	31.93	31.78	32.28	34.12	35.57	34.98	35.34
	33.77	33.85	33.79	34.15	35.16	35.34	35.36	36.70	35.95	36.69
	34.93	35.02	34.95	37.89	39.98	40.51	38.68	39.28	41.15	39.17
Nikon D800 ISO = 1600	35.47	35.54	35.57	33.77	34.84	35.09	37.34	38.01	37.99	38.82
	35.71	35.79	35.77	35.89	38.42	38.65	38.57	39.05	40.36	40.98
	34.81	34.92	34.95	34.25	35.79	35.85	37.87	38.20	38.30	38.90
Nikon D800 ISO = 3200	33.26	33.34	33.31	37.42	38.36	38.56	36.95	38.07	39.01	38.69
	32.89	32.95	32.96	34.88	35.53	35.76	35.09	35.72	36.75	36.82
	32.91	32.98	32.96	38.54	40.05	40.59	36.91	36.76	39.06	38.80
Nikon D800 ISO = 6400	29.63	29.66	29.71	33.59	34.08	34.25	31.28	33.49	34.61	33.31
	29.97	30.01	29.98	31.55	32.13	32.38	31.38	32.79	33.21	33.18
	29.87	29.90	29.95	31.42	31.52	31.76	31.40	32.86	33.22	33.35
Average PSNR	33.41	33.48	33.48	34.32	35.33	35.65	35.49	36.43	36.88	37.26
Average SSIM	0.8483	0.8511	0.8512	0.9113	0.9250	0.9280	0.9126	0.9364	0.9481	0.9505

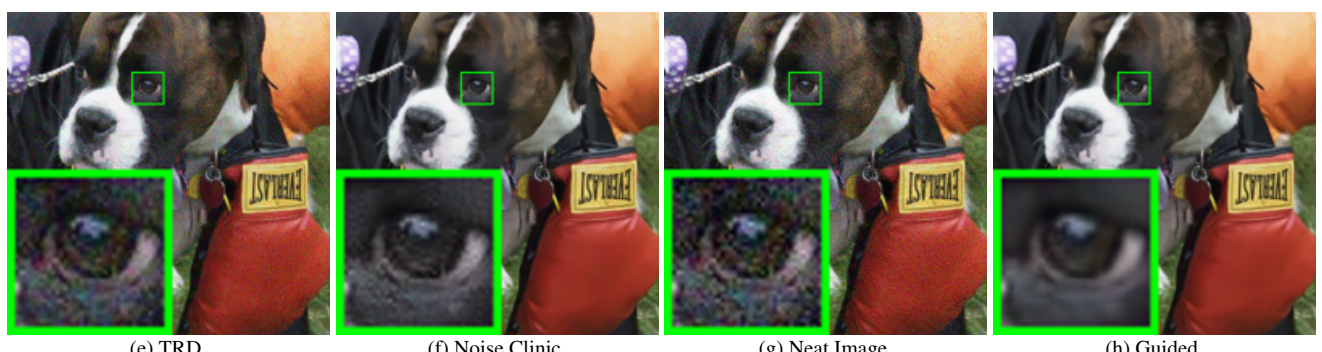
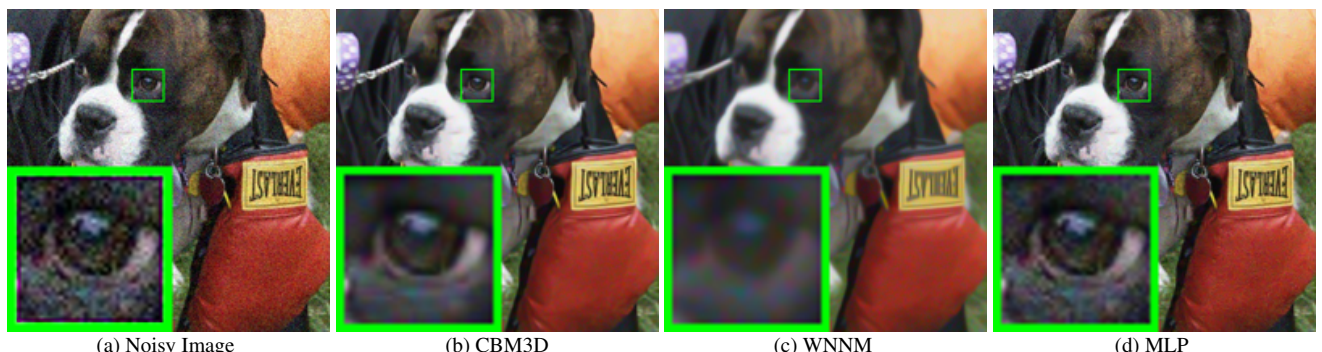
- [784] [15] J. Portilla. Full blind denoising through noise covariance
785 estimation using gaussian scale mixtures in the wavelet do-
786 main. *Image Processing, 2004. ICIP '04. 2004 International
787 Conference on*, 2:1217–1220, 2004. 1, 3
- [788] [16] Tamer Rabie. Robust estimation approach for blind denoising.
789 *Image Processing, IEEE Transactions on*, 14(11):1755–
790 1765, 2005. 1, 3
- [791] [17] C. Liu, R. Szeliski, S. Bing Kang, C. L. Zitnick, and W. T.
792 Freeman. Automatic estimation and removal of noise from
793 a single image. *IEEE Transactions on Pattern Analysis and
794 Machine Intelligence*, 30(2):299–314, 2008. 1, 3
- [795] [18] Zheng Gong, Zuowei Shen, and Kim-Chuan Toh. Image
796 restoration with mixed or unknown noises. *Multiscale Mod-
797eling & Simulation*, 12(2):458–487, 2014. 1, 3
- [798] [19] M. Lebrun, M. Colom, and J.-M. Morel. Multiscale image
799 blind denoising. *Image Processing, IEEE Transactions on*,
800 24(10):3149–3161, 2015. 1, 2, 3, 5
- [801] [20] Fengyuan Zhu, Guangyong Chen, and Pheng-Ann Heng.
From noise modeling to blind image denoising. *The IEEE
803 Conference on Computer Vision and Pattern Recognition
804 (CVPR)*, June 2016. 1, 3
- [805] [21] C. M. Bishop. *Pattern recognition and machine learning*.
806 New York: Springer, 2006. 1
- [807] [22] Z. Wang, A. C. Bovik, H. R. Sheikh, and E. P. Simoncelli.
808 Image quality assessment: from error visibility to struc-
809

tural similarity. *IEEE Transactions on Image Processing*,
13(4):600–612, 2004. 1, 6

- [810] [23] K. Dabov, A. Foi, V. Katkovnik, and K. Egiazarian. Color
811 image denoising via sparse 3d collaborative filtering with
812 grouping constraint in luminance-chrominance space. *IEEE
813 International Conference on Image Processing*, 1, 2007. 2
- [814] [24] Neatlab ABSoft. Neat image. [https://ni.
815 neatvideo.com/home](https://ni.neatvideo.com/home). 2, 3, 5
- [816] [25] G. Yu, G. Sapiro, and S. Mallat. Solving inverse problems
817 with piecewise linear estimators: From Gaussian mixture
818 models to structured sparsity. *IEEE Transactions on Image
819 Processing*, 21(5):2481–2499, 2012. 2, 3
- [820] [26] Daniel Glasner, Shai Bagon, and Michal Irani. Super-
821 resolution from a single image. *ICCV*, 2009.
- [822] [27] Maria Zontak, Inbar Mosseri, and Michal Irani. Separating
823 signal from noise using patch recurrence across scales. *Pro-
824 ceedings of the IEEE Conference on Computer Vision and
825 Pattern Recognition*, pages 1195–1202, 2013.
- [826] [28] Tomer Michaeli and Michal Irani. Blind deblurring using in-
827 ternal patch recurrence. *European Conference on Computer
828 Vision*, pages 783–798, 2014.
- [829] [29] Y. Bahat and M. Irani. Blind dehazing using internal patch
830 recurrence. *IEEE International Conference on Computa-
831 tional Photography (ICCP)*, pages 1–9, May 2016.



885 Figure 6. Denoised images of the image "Canon 5D Mark 3 ISO 3200 1" by different methods. The images are better to be zoomed in on screen.



910 Figure 7. Denoised images of the image "5dmak3iso32003" by different methods. The images are better to be zoomed in on screen.

911 [30] J. Portilla, V. Strela, M.J. Wainwright, and E.P. Simoncelli.
912 Image denoising using scale mixtures of Gaussians in the
913 wavelet domain. *Image Processing, IEEE Transactions on*,
914 12(11):1338–1351, 2003. 3

[31] Peter J Huber. *Robust statistics*. Springer, 2011. 3

[32] M. Lebrun, A. Buades, and J. M. Morel. A nonlocal bayesian
915 image denoising algorithm. *SIAM Journal on Imaging Sciences*,
916 6(3):1665–1688, 2013. 3

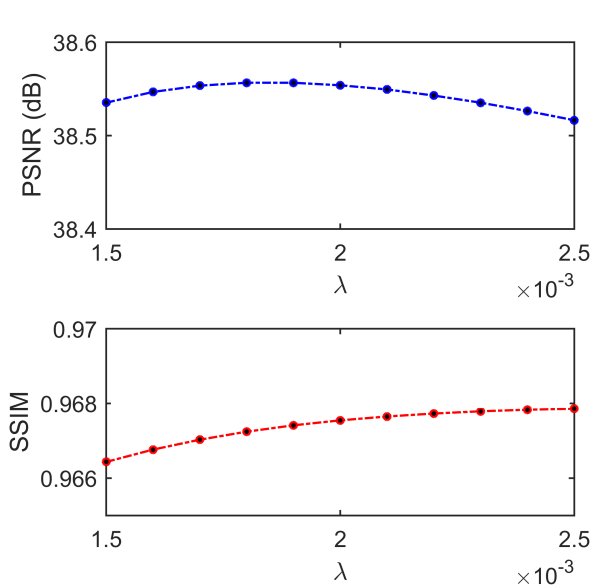


Figure 8. The PSNR/SSIM results as a function of the parameter λ .

- [33] W. Dong, L. Zhang, G. Shi, and X. Li. Nonlocally centralized sparse representation for image restoration. *Image Processing, IEEE Transactions on*, 22(4):1620–1630, 2013. 2, 3
- [34] Chenglong Bao, Jian-Feng Cai, and Hui Ji. Fast sparsity-based orthogonal dictionary learning for image restoration. *Proceedings of the IEEE International Conference on Computer Vision*, pages 3384–3391, 2013. 4
- [35] A. P. Dempster, N. M. Laird, and D. B. Rubin. Maximum likelihood from incomplete data via the EM algorithm. *Journal of the Royal Statistical Society. Series B (methodological)*, pages 1–38, 1977. 4
- [36] David L Donoho and Michael Elad. Optimally sparse representation in general (nonorthogonal) dictionaries via 1 minimization. *Proceedings of the National Academy of Sciences*, 100(5):2197–2202, 2003. 4
- [37] Franklin C. Crow. Summed-area tables for texture mapping. *SIGGRAPH Comput. Graph.*, 18(3):207–212, January 1984. 5
- [38] Paul Viola and Michael J Jones. Robust real-time face detection. *International journal of computer vision*, 57(2):137–154, 2004. 5
- [39] S. Osher, M. Burger, D. Goldfarb, J. Xu, and W. Yin. An iterative regularization method for total variation-based image restoration. *Multiscale Modeling & Simulation*, 4(2):460–489, 2005. 5